POLITECNICO DI TORINO
Repository ISTITUZIONALE

Intima-Media Thickness: Setting a Standard for a Completely Automated Method of Ultrasound Measurement

(Article begins on next page)

05 August 2020

Intima-Media Thickness: Setting a Standard for a Completely Automated Method of Ultrasound Measurement

Filippo Molinari, *Member, IEEE*, Guang Zeng, and Jasjit S. Suri, *Senior Member, IEEE*

Abstract—The intima-media thickness (IMT) of the common carotid artery is a widely used clinical marker of severe cardiovascular diseases. IMT is usually manually measured on longitudinal B-mode ultrasound images. Many computer-based techniques for IMT measurement have been proposed to overcome the limits of manual segmentation. Most of these, however, require a certain degree of user interaction.

In this paper we describe a new, completely automated layer extraction technique (named CALEXia) for the segmentation and IMT measurement of the carotid wall in ultrasound images. CALEXia is based on an integrated approach consisting of feature extraction, line fitting, and classification that enables the automated tracing of the carotid adventitial walls. IMT is then measured by relying on a fuzzy K-means classifier. We tested CALEXia on a database of 200 images. We compared CALEXia's performance with those of a previously developed methodology that was based on signal analysis (CULEXsa). Three trained operators manually segmented the images and the average profiles were considered as the ground truth. The average error from CALEXia for lumen-intima (LI) and media-adventitia (MA) interface tracings were 1.46 ± 1.51 pixel (0.091 ± 0.093 mm) and 0.40 ± 0.87 pixel (0.025 ± 0.055 mm), respectively. The corresponding errors for CULEXsa were 0.55 ± 0.51 pixels (0.035 ± 0.032 mm) and 0.59 ± 0.46 pixels (0.037 ± 0.029 mm). The IMT measurement error was equal to 0.87 ± 0.56 pixel (0.054 ± 0.035 mm) for CALEXia and 0.12 ± 0.14 pixel (0.01 ± 0.01 mm) for CULEXsa. Thus, CALEXia showed limited performance in segmenting the LI interface, but outperformed CULEXsa in the MA interface and in the number of images correctly processed (190 for CALEXia and 184 for CULEXsa). Based upon two complementary strategies, we anticipate fusing them for further IMT improvements.

I. Introduction

THE atherosclerotic process refers to the deposit of lipids in the artery wall. The increase of the artery walls thickness causes a reduction of the lumen with possible vascular problems. The increase in the intima-media thickness (IMT) of the carotid artery is one of the earlier clinical signs of an ongoing atherosclerotic process [1]. It has been shown that atherosclerosis increases the risk of several pathologies, ranging from myocardial infarction to stroke [2].

The IMT measurement is usually performed by relying on ultrasound images. The ultrasound technique produces images with lower spatial resolution and signal-to-noise ratio when compared with other imaging modalities, such as angiography, multi-slice computer tomography (CT), and magnetic resonance imaging (MRI). However, angiography and CT expose the patient to radiation and require injection of contrast agents, whereas MRI is time consuming and technically challenging [3]. In addition, X-ray angiography, CT, and MRI have high associated costs compared with ultrasound. Because ultrasound devices are cheap, portable, real-time, and use no ionizing radiation, IMT is usually measured on B-mode ultrasound images in clinical practice.

Manual measurement of the IMT by expert sonographers is highly reliable but time consuming. Also, results depend on the expert, with associated subjectivity. Therefore, manual segmentation is impractical in large studies where standardization of the protocol is required and where the number of patients is very high.

Different techniques have been proposed to perform automated IMT segmentation. Some techniques were intended as computer-aided systems to help the operator in the measurement process [4] and required human interaction. Methods based on edge-detectors [5] usually require the manual selection of the carotid artery in the image frame. Dynamic programming techniques [6] are often device-dependent and require retraining when the image characteristics change. Snake-based algorithms [7], [8] have a problem in initialization: the snake cannot reach a satisfactory convergence if its initial contour is placed far from the artery layers. Therefore, most of the snake-based methodologies are driven by the user. Human intervention precludes real automation and biases the results.

Recently, Golemati *et al.* proposed an automated technique for the carotid segmentation and IMT measurement which was based on the Hough transform [9]. This algorithm could locate the common carotid artery (CCA) both in longitudinal and transverse images without any user interaction. The challenge with this technique is that only vessels appearing as horizontal and straight can be correctly identified and processed. However, B-mode images depicting a curved CCA or an inclined vessel are common in clinical practice. Another characteristic of this methodology is the need for human interaction to calculate the IMT.

In 2007, the authors developed a completely user-independent technique for the carotid artery wall segmenta-

tion [10]. Our methodology (CULEXsa: completely user-independent layer extraction based on signal analysis) was effective in processing both normal and diseased carotids, but suffered from the problem of noise and image artifacts. This resulted in a failure rate of about 15% of the images. Moreover, being based on local statistics, real-time implementation was impossible because of computational cost. Nevertheless, segmentation performances were satisfactory. When compared with manual tracings made by experts, the system gave segmentation errors lower than 1 pixel (corresponding to about 0.06 mm) on the lumen-intima (LI) and media-adventitia (MA) boundaries. The error on the IMT measurement was about 56 µm [10], [11]. The final segmentation step of CULEXsa is snake-based; hence, CULEXsa shares most of the limitations that affect the other snake-based methodologies.

To overcome the limitations of this technique, in 2009 we developed a completely automatic method for the CCA localization in longitudinal B-mode images [12]. We named this technique CALEXia (completely automatic layer extraction based on integrated approach). This unique methodology was based on an integrated approach consisting of feature extraction, line fitting, and classification. We tested CALEXia on a 200-image database and validated its performance against human tracings. We showed that CALEXia can trace the near and far adventitial layers with average errors of about 70 µm for the near adventitia and 170 µm for the far adventitia. The major advantages of this novel technique are: 1) user-independence, 2) reduced computational cost, 3) suitability for normal as well as pathological images, and 4) the correct processing of any anatomy of the CCA (i.e., curved, inclined, or diseased vessels).

The aim of this study was twofold: 1) to extend CALEXia for IMT measurement and validation; and 2) to compare CALEXia with CULEXsa on the same image database and to set a standard of care for IMT measurement in a clinical setting. Thus, our goal was to develop a robust utility for CCA segmentation and IMT measurement in diverse pathological cases.

II. MATERIALS AND METHODS

A. Image Database and Recording Equipment

B-mode images of the common tract of the carotid artery were acquired by an ATL HDI500 device (ATL Ultrasound, Seattle, WA) equipped with a linear probe (code L12–5) with 38 mm aperture, 192 elements, and working in the frequency range of 5 to 12 MHz. All the images were acquired at a frequency of 10 MHz. Focal position was adjusted according to the depth of the CCA and resulted in a range of 2.5 to 5 cm. Considering a ultrasound propagation velocity equal to 1550 m/s, the resultant wavelength was equal to 155 µm. All the images were log-compressed and transferred to a computer via a DICOM communication module. Because clinicians adjusted the scanning

depth to anatomy during acquisitions, we resampled all the images at a standard density of 16 pixels/mm [8], [13]. Axial resolution on the digitized image was thus equal to 0.0625 mm. All the images were coded by a 256-level grayscale (8-bit). We did not impose a standard gain setting for all the acquisitions; in fact, the sonographer was instructed to adjust the gain settings according to his expertise and to best practice. This was done to test the strength of our techniques on real acquired data.

Our testing database consisted of 200 images acquired from 150 consecutive patients (age 50 to 83 years; mean $\pm$ standard deviation $= 69 \pm 16$ years) of the Neurology Division of the Gradenigo Hospital, Torino, Italy. Ninety subjects were males. All of the subjects were symptomatic and were referred to the Neurology Division either for neurological or cardiovascular disorders. All of the subjects were instructed about the study and signed an informed consent form prior to being submitted to the ultrasound examination. The Institutional Committee of the Gradenigo Hospital approved this study.

B. Architecture of CULEXsa

CULEXsa is a completely user-independent algorithm for extracting the layers of the artery wall. It is a two-step procedure based on signal analysis that:

1) Automatically traces the near (AD_N) and far (AD_F) adventitia profiles;
2) Starting from the detected far adventitia, it adopts a gradient-based segmentation followed by a snake refinement to trace the lumen-intima (LI) and media-adventitia (MA) boundaries.

The detailed structure of CULEXsa has already been described [10], [11]. Recently, we also demonstrated that CULEXsa is effective in detecting the CCA in normal as well as pathological images and that its performances are independent of the ultrasound OEM scanner used for data acquisition [14].

We summarize the overall functioning of CULEXsa as follows:

1) The automated procedure for the recognition of the CCA in the image is based on local statistics. Carotid characteristics can be thought of as a mixture model with varying characteristics. This is because a) pixels belonging to the vessel L are characterized by low mean intensity and homogeneous neighborhood; b) pixels belonging to the adventitia layer are characterized by a high mean intensity and a homogeneous neighborhood; c) all remaining pixels should have average mean intensity and non-homogeneous neighborhood. Therefore, for each pixel of the image, we compute the mean and standard deviation of a 10×10 neighborhood. Mean values and standard deviation values are grouped into a histogram, where each class has a width equal to 0.02 [14]. We dem-
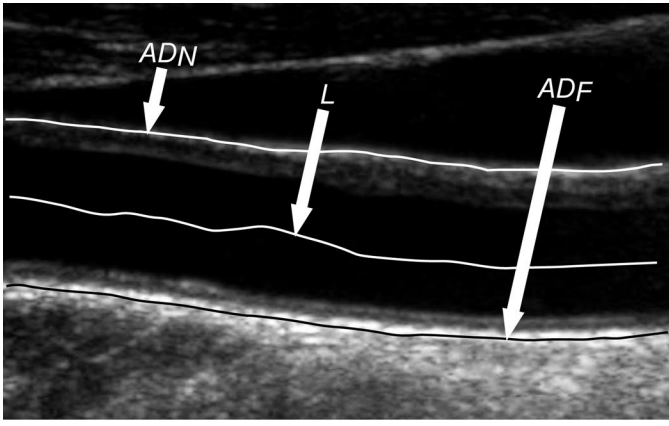
Fig. 1. Automated common carotid artery detection performed by CULEXsa. The algorithm traces the profiles of the near (AD_N) and far (AD_F) adventitia. It also traces the course of the vessel lumen (L).
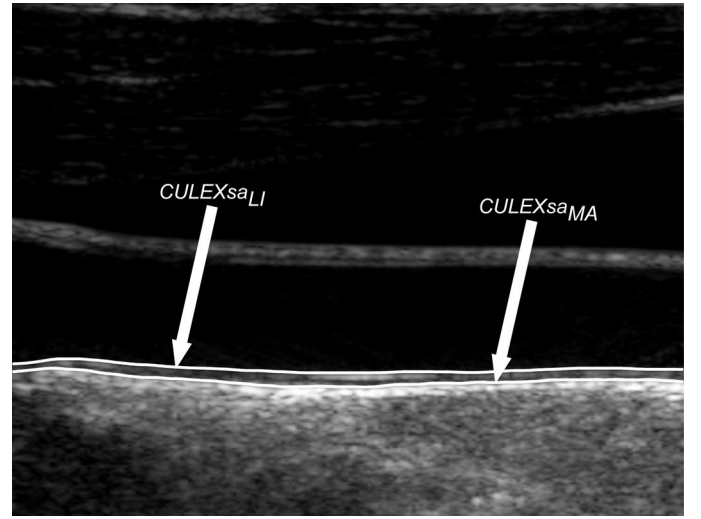

Fig. 2. Image segmentation performed by CULEXsa: $CULEXsa_{LI}$ denotes the lumen-intima tracing; $CULEXsa_{MA}$ denotes the media-adventitia tracing.

onstrated that pixels belonging to the carotid lumen have mean intensity lower than 0.08 and standard deviation lower than 0.14 [14].

2) Once the bi-dimensional histogram has been calculated, the image is scanned column-wise. For each column, by using the signal envelope of the intensity profile, we first detect the AD_F layer, which is the brightest local maximum that can be found starting from the bottom of the image (i.e., from the highest row-index). Then, we search for a minimum local intensity whose neighborhood mean intensity is lower than 0.08 and standard deviation is lower than 0.14. This point was assigned to the L. At this point, the row-index is decreased and the first local intensity maxima is taken as the AD_N. The sequence of all the detected points forms the AD_N, AD_F, and L profiles. An example of CULEXsa automated detection of the CCA is shown in Fig. 1.

3) Only the pixels between the AD_F and the L profiles (with reference to Fig. 1) are considered. For each column of the image, using the gradient approach we performed a first estimate of the LI and MA profiles. The two higher intensity maxima of the gradient were considered as the initial guess of the LI and MA interfaces. The sequence of the detected points in all the columns formed the initial guess of the lumen LI and MA profiles.

4) Finally, the LI and MA profiles are refined by using a snake algorithm. We adopted the classical formulation of the energy function as proposed by Williams and Shah [15]. The same formulation has been widely used in other studies [7], [8], [16]. Based on previous experience [10], we choose the following smoothing coefficients for the snake parameters: $\alpha(s) = 0.1$ and $\beta(s) = 0.01$.

Fig. 2 shows a sample of CULEXsa segmentation of a CCA image. Full details can be seen in [10], [11].

C. Architecture of CALEXia

CALEXia was developed as a generalized architecture for vessel wall segmentation. In this study, we specifically developed the segmentation of the distal (far) CCA wall, where the measurement of the IMT is more reliable. CALEXia consists of two parts:

1) a module that automatically locates the CCA in the image;
2) a segmentation procedure that automatically traces the LI and the MA contours of the distal (far) wall once CCA has been localized.

Part 1 of CALEXia architecture is the tracing of the distal and proximal adventitia layers. An example of the CALEXia recognition procedure of the CCA shown in Fig. 3. The original B-mode image [Fig. 3(a)] is considered column-wise after a heavy downsampling of the columns number. For each column, the algorithm finds qualified local intensity maxima that are located on the adventitial walls. These points are called seed points [seed points are overlaid on the grayscale image shown in Fig. 3(b)]. To estimate the location of the adventitial walls, seed points are then linked to form line segments. Line segments are then connected if they are closed, adjacent, and aligned, therefore avoiding over-segmentation of the adventitial walls. Line segments that do not lie over features of the image are discarded. This ensures that only highly echogenic image features are recognized. Valid line segments for the image in Fig. 3(a) are shown in Fig. 3(c) (they are denoted LS_1, LS_2, and LS_3). Among all the valid line segments, the procedure finds the pair that has the higher probability of enclosing the vessel lumen: if the pixel comprised between the two line segments are of low intensity and homogeneous, then the line segments correspond to the adventitia layers of the artery. In Fig. 3(c), the correct
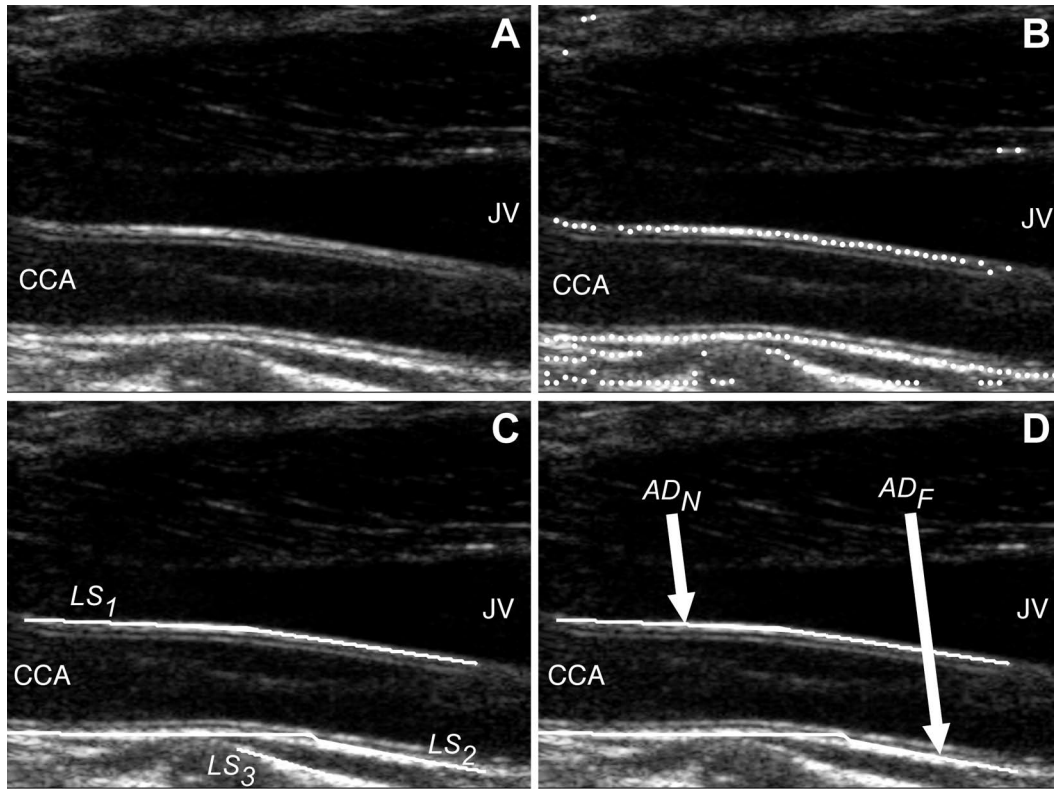
Fig. 3. Overview of the CALEXia segmentation strategy for common carotid artery (CCA) localization. (A) Original B-mode image of the common tract of the carotid artery (JV is the jugular vein). (B) White dots represent the seed points detected on the image. These points are local intensity maxima. They constitute the basis for tracing line segments. (C) Line segments after fitting. LS_1, LS_2, and LS_3 represent the line segments that the procedure traced starting from the seed points. (D) Final tracings of the near and proximal (AD_N) and of the far and distal (AD_F) adventitia. This final tracing is derived from the line segments in (B) after classification.

line segments are LS_1 and LS_2. The identified line segments become the final tracings of the adventitia layers [Fig. 3(d)]. The mathematical aspects of the first part of CALEXia are detailed in [12].

The innovative aspect of this study is the usage of CALEXia as a segmentation technique (i.e., its completion with part 2, as described previously). The segmentation strategy consists of the following steps:

1) To attenuate the effect of noise, we low-pass filter the image by using a 5×5 pixel Gaussian kernel with zero mean and standard deviation equal to 1.

2) We identify a region of interest (ROI) starting from the traced far adventitia profile [indicated by AD_F in Fig. 4(a)]. The width of the ROI is taken equal to the support of the AD_F tracing. The upper limit of the ROI is calculated by moving the points of the AD_F boundary 20 pixels (1.25 mm) in the vertical direction (i.e., toward the CCA lumen). The lower limit of the ROI is calculated by shifting the AD_F points 10 pixels (0.625 mm) downward (i.e., toward the bottom of the image). We chose these shift values to ensure that the ROI comprised a portion of the CCA lumen and the tissues underneath the CCA. This ROI definition is robust even in presence of curved vessels. An example of the resultant ROI is

shown by the area enclosed by the white dashed line in Fig. 4(b).

3) We process only the pixels in the ROI. The ROI is considered column-wise. For each column we extract the signal envelope corresponding to the vertical intensity profile. In Fig. 4(c), the white dashed line indicates a column of the ROI and the black line in Fig. 4(d) represents the signal envelope. We consider only the pixels between the row-index 0 and the row-index corresponding to the position of the adventitial layer [in Fig. 4(d) the AD_F position is indicated by the vertical black dashed line. The corresponding row-index is 37].

4) The points of the signal envelope comprised between 0 and the AD_F are clustered by using a fuzzy K-means classifier. We fix the number of classes equal to three, ideally: artery lumen, intima-media complex, and adventitia layer. The classifier uses a Euclidean distance metric. Initialization is done by feeding the gray level intensity values along the signal envelope as input. Artery lumen, intima and media layers, and adventitial layer can be easily identified by sorting the center value of each class. The pixels at the boundaries between the clusters are considered as the markers of the LI and MA interfaces. The black dots in Fig. 4(d) overlaid on the signal envelope in-
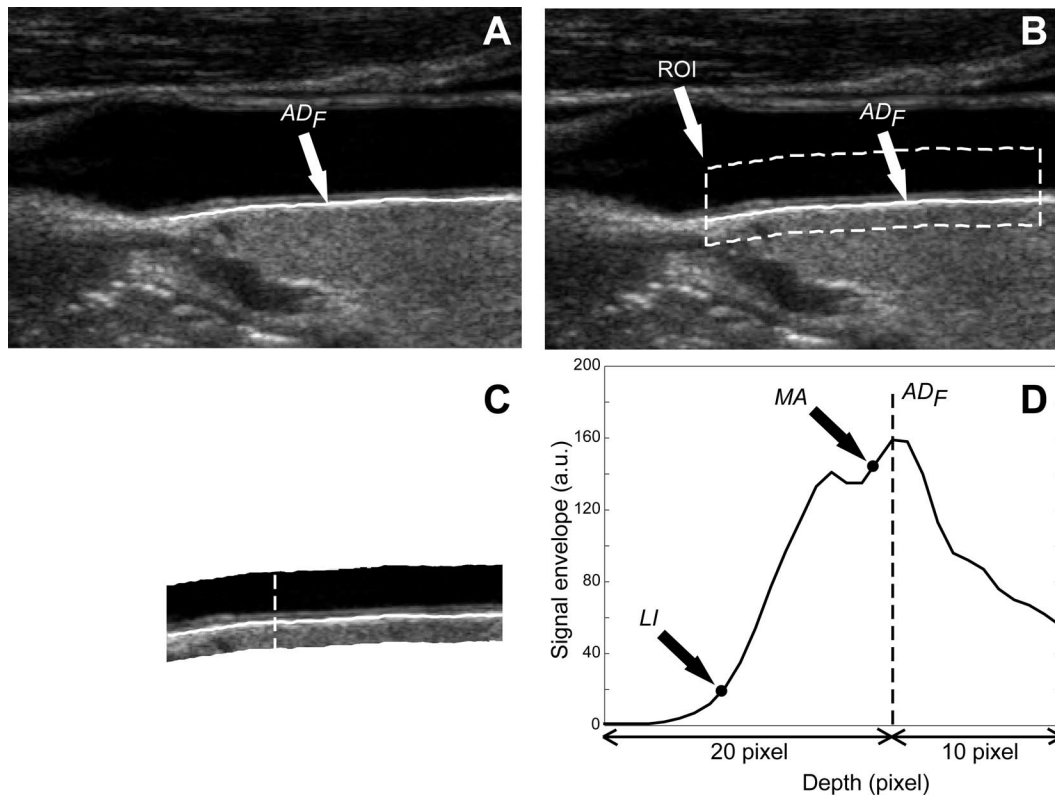
Fig. 4. Schematic representation of segmentation performed by CALEXia. (A) Original image with far adventitia tracing (AD_F). The AD_F represent the starting point of the segmentation procedure. (B) Automatic ROI tracing based on the AD_F profile. The ROI width is the same as AD_F tracing. The upper limit of the ROI is set by shifting the AD_F profile 20 pixels (1.25 mm) upward. The lower limit of the ROI is set by shifting the AD_F profile 40 pixels (2.5 mm) downward. (C) The previously extracted ROI is the only portion of the image that is segmented. The pixels are considered column-wise (the white dashed line indicates one column of the ROI). (D) The signal envelope of the intensity profile calculated along the white dashed line in (C). The horizontal axis reports the index row (i.e., the depth of the image, depth increases toward the right end of the graph). The vertical axis reports the signal envelope amplitude in arbitrary units. The vertical dashed line marks the position of the far adventitia. The black circles represent the boundaries between lumen-intima (LI) and media-adventitia (MA) detected by the fuzzy K-means classifier.

dicate the position of the detected LI and MA interfaces.

5) Steps 3 and 4 are repeated for all the columns of the ROI. If the classifier fails to find 3 contiguous regions in a given column, then we discard that column. The sequence of the identified LI and MA markers constitute the final segmentation of the CCA wall. The final profiles are then regularized by a B-spline. The result of the segmentation process for the image in Fig. 4(a) is shown in Fig. 5.

The two approaches we developed are based on completely different strategies. In CULEXsa we exploit the local statistics of the image pixels to automatically discriminate between lumen pixels and tissue pixels. Pixels are considered as possibly belonging to the carotid lumen if their intensity is low and if other low-intensity points surround them. When the algorithm scans the intensity profile of each column, the local statistic is recalled as a stopping criterion: in fact, the markers of the adventitia walls are found as local maxima provided lumen pixels separate them. Therefore, our local statistics is basically inspired by the artery morphology and by the human perception of the carotid artery in the ultrasound frame. This enables
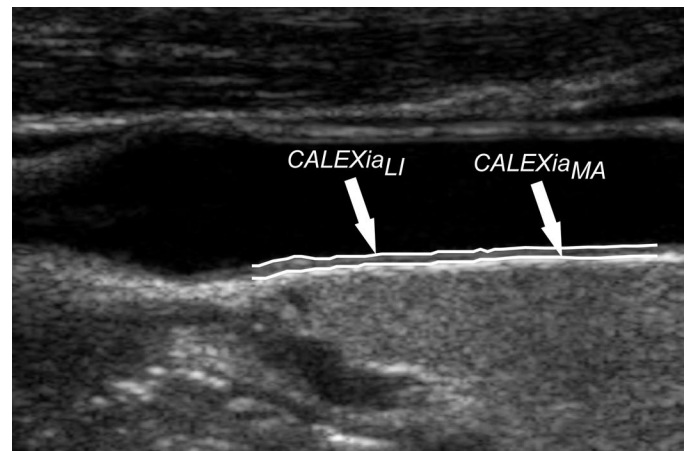
Fig. 5. Image segmentation performed by CALEXia. The image is the same as in Fig. 4(A). CALEXia$_{LI}$ represents the lumen-intima tracing. CALEXia$_{MA}$ represents the media-adventitia tracing.

the automated localization of the CCA in the B-mode image. The CULEXsa segmentation process is based on a combination of gradient and snake paradigms.

On the other hand, the CALEXia strategy is based on an integrated approach of feature extraction, line fitting, and classification. The feature extraction procedure is

needed to select what we called seed points. These points constitute the basis of both the automated CCA localization and of the segmentation. Seed points are local intensity maxima with specific characteristics (intensity value and breadth of the intensity curve) that are on the carotid walls (and specifically on the adventitia layer, which is the most echogenic part of the artery wall). True seed points are selected among candidates by using intelligent approaches based on linear discriminators that were trained in a previous study [12]. By connecting the seed points and classifying the resulting line segments, the adventitia layers of the CCA can be easily traced. Using fuzzy logic, we performed the segmentation of the LI and MA boundaries in CALEXia.

Therefore, although they are both completely user-independent techniques, CULEXsa and CALEXia exploit totally different image features. This study compares their performance in terms of CCA segmentation and IMT measurement.

D. Performance Evaluation Metrics

We developed a graphical user interface for three expert operators (a physician, a technician, and a neurologist), which they used independently to segment all of the 200 images in the testing database [11]. We considered as ground truth (GT) to be the average profile of the human tracings.

Considering the ith image in the database, we defined the segmentation error for each column c of the image as

$$\varepsilon^i_{\text{CALEXia}_{\text{LI}}}(c) = \left| \text{CALEXia}^i_{\text{LI}}(c) - \text{GT}^i_{\text{LI}}(c) \right|$$
$$\varepsilon^i_{\text{CALEXia}_{\text{MA}}}(c) = \left| \text{CALEXia}^i_{\text{MA}}(c) - \text{GT}^i_{\text{MA}}(c) \right|, \quad (1)$$

where $\varepsilon^i_{\text{CALEXia}_{\text{LI}}}$ and $\varepsilon^i_{\text{CALEXia}_{\text{MA}}}$ represent CALEXia's absolute segmentation errors for the LI and MA interfaces, respectively; $\text{CALEXia}^i_{\text{LI}}$ and $\text{CALEXia}^i_{\text{MA}}$ represent the LI and MA profiles as traced by CALEXia; GT^i_{LI} and GT^i_{MA} represent the LI and MA GT profiles; and c is an index spanning the columns of the image. Using this nomenclature, we mathematically represented the errors for the CULEXsa algorithm as

$$\varepsilon^i_{\text{CULEXsa}_{\text{LI}}}(c) = \left| \text{CULEXsa}^i_{\text{LI}}(c) - \text{GT}^i_{\text{LI}}(c) \right|$$
$$\varepsilon^i_{\text{CULEXsa}_{\text{MA}}}(c) = \left| \text{CULEXsa}^i_{\text{MA}}(c) - \text{GT}^i_{\text{MA}}(c) \right|, \quad (2)$$

where $\text{CULEXsa}^i_{\text{LI}}$ and $\text{CULEXsa}^i_{\text{MA}}$ represent the LI and MA profiles as traced by CULEXsa.

We also adopted the percent statistic algorithm to test whether the computer-generated boundaries differ from manual tracings as much as the manual tracings differ from one another. This test was proposed by Chalana *et al.* [17] and then modified by Alberola-Lòpez *et al.* [18]. The basic idea is that if the computer-generated boundary behaves like a human-generated boundary, it must have the same probability of falling within the inter-observer

range as the manual segmentation. For each tracing C_i, we computed the distance D_{ij} from any other contour C_j. As proposed in previous studies, we used the average distance metric [18]. Let D_m be the maximum distance between any two tracings (i.e., $D_m = \max_{i,j}\{D_{ij}\}$ for $i \neq j$). A tracing falls in the inter-observer range if the distances separating it from the others tracings are all lower than D_m. Assuming the human tracings as independent and identically distributed, the probability p of the computer-generated boundary falling into the inter-observer range is equal to $p = (n - 1)/(n + 1)$, where $n + 1$ is the total number of tracings (i.e., n human tracing and 1 computer-generated boundary; in our study $n = 3$) and $n - 1$ is the number of contours minus the two contours with distance D_m. Defining X_j as the event "the computer-generated tracing lies within the inter-observer range for the jth image," then X_j is a random variable with Bernoulli distribution of parameters p and $q = 1 - p$. Because we have a database consisting of $n = 200$ images, the variable $Z = \sum_{j=1}^{N} X_j/N$ can be considered as normally distributed with mean value equal to p and standard deviation equal to pq/N. Because we are trying to determine whether the computer-generated tracing falls outside the inter-observer range more often than the human tracings, we seek the one-sided confidence interval for the variable Z, i.e., the θ value for which $P(p - Z > \theta) = \alpha$, where $1 - \alpha$ is the significance level. It was shown that $\theta = \sqrt{pq/N} z_{1-\alpha}$ [18], where $z_{1-\alpha}$ is the value of a normal standard variable leaving an area equal to $1 - \alpha$ to its right. Therefore, the acceptance region for this test is where the critical value Z_0 is greater than $p - \theta$.

Finally, the IMT measurement was defined for the automated techniques and for the manual segmentations as follows:

$$\text{CALEXia}^i_{\text{IMT}}(c) = \text{CALEXia}^i_{\text{MA}}(c) - \text{CALEXia}^i_{\text{LI}}(c)$$
$$\text{CULEXsa}^i_{\text{IMT}}(c) = \text{CULEXsa}^i_{\text{MA}}(c) - \text{CULEXsa}^i_{\text{LI}}(c) \quad (3)$$
$$\text{GT}^i_{\text{IMT}}(c) = \text{GT}^i_{\text{MA}}(c) - \text{GT}^i_{\text{LI}}(c),$$

where $\text{CALEXia}^i_{\text{IMT}}$ and $\text{CULEXsa}^i_{\text{IMT}}$ are the IMT measurements of CALEXia and CULEXsa and GT^i_{IMT} is the IMT measurement derived by ground truth profiles.

With the mathematical expression of IMT given in (3), we defined the IMT measurement errors for CALEXia and CULEXsa as

$$\varepsilon^i_{\text{CALEXia}_{\text{IMT}}}(c) = \left| \text{CALEXia}^i_{\text{IMT}}(c) - GT^i_{IMT}(c) \right|$$
$$\varepsilon^i_{\text{CULEXsa}_{\text{IMT}}}(c) = \left| \text{CULEXsa}^i_{\text{IMT}}(c) - GT^i_{IMT}(c) \right|, \quad (4)$$

where $\varepsilon^i_{\text{CALEXia}_{\text{IMT}}}$ and $\varepsilon^i_{\text{CULEXsa}_{\text{IMT}}}$ represent the CALEXia and CULEXsa absolute IMT measurement error for the ith image. The index c spans the columns of the image.

III. Results and Data Analysis

In the following, we illustrate the segmentation performance of CALEXia and compare it with CULEXsa.
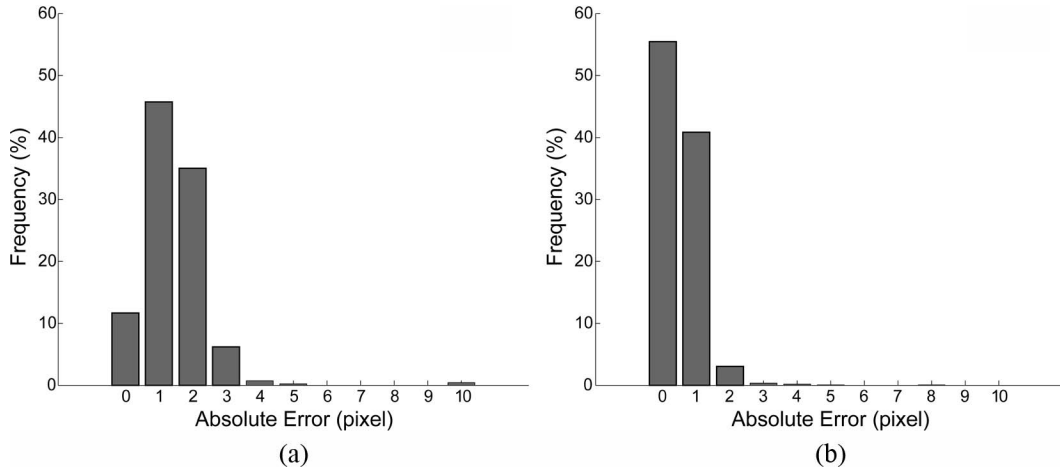
Fig. 6. Absolute segmentation error distributions of the LI profiles for CALEXia and CULEXsa. The 9100 error values (50 points × 182 images) are grouped in classes of 1 pixel each. The horizontal axis reports the absolute error in pixels. The vertical axis reports the relative frequency (i.e., the number of points falling in each class expressed as a percentage of the total number of error values). (a) Distribution of $\varepsilon^i_{\mathrm{CALEXia_{LI}}}$. (b) Distribution of $\varepsilon^i_{\mathrm{CULEXsa_{LI}}}$.
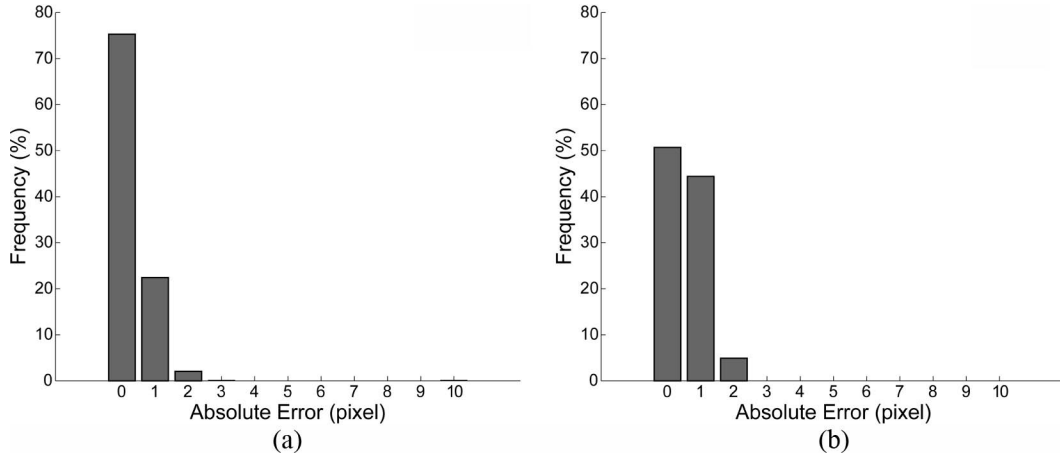

Fig. 7. Absolute segmentation error distributions of the MA profiles for CALEXia and CULEXsa. The 9100 error values (50 points × 182 images) are grouped in classes of 1 pixel each. The horizontal axis reports the absolute error in pixels. The vertical axis reports the relative frequency (i.e., the number of points falling in each class expressed as a percentage of the total number of error values). (a) Distribution of $\varepsilon^i_{\mathrm{CALEXia_{MA}}}$. (b) Distribution of $\varepsilon^i_{\mathrm{CULEXsa_{MA}}}$.

Of the 200 images, CALEXia could not correctly identify the CCA in 10 images (5% of the images). We previously discussed the possible problems of CALEXia in automatic detection of the artery [12]. In these 10 images, CALEXia detected the jugular vein instead of the carotid artery; these images were removed from the database.

CULEXsa could not process 16 images out of 200 (8% of the images) because of excessive noise that precluded a proper identification of the far adventitia layer. Eight images were among the images that CALEXia could not process. Therefore, we removed 18 images from the database and tested our algorithms on $n = 182$ images.

A. Near and Far Carotid Profiles and Segmentation Error

For each image, we first computed the common support between GT, CALEXia, and CULEXsa. Then, we calcu-

lated the absolute segmentation errors in 50 equally spaced points. Thus, we obtained 9100 absolute error values for each interface and for each technique according to (1) and (2). Fig. 6 depicts the errors of the LI interface: the distributions of the CALEXia error $\left(\varepsilon^i_{\mathrm{CALEXia_{LI}}}\right)$ are reported by Fig. 6(a), whereas Fig. 6(b) reports the distribution of the CULEXsa errors $\left(\varepsilon^i_{\mathrm{CULEXsa_{LI}}}\right)$. The horizontal axis represents the error expressed in pixels, the vertical axis reports the relative frequency as a percentage. The mean error for the LI interface is equal to 1.46 ± 1.51 pixels for CALEXia and to 0.55 ± 0.51 pixels for CULEXsa.

Fig. 7 reports the errors for the MA interface. The distribution of the CALEXia errors $\varepsilon^i_{\mathrm{CALEXia_{MA}}}$ is shown in Fig. 7(a); whereas Fig. 7(b) depicts the CULEXsa errors $\varepsilon^i_{\mathrm{CULEXsa_{MA}}}$. The mean error for the MA interface is equal to 0.40 ± 0.87 pixels for CALEXia and 0.59 ± 0.46 pixels
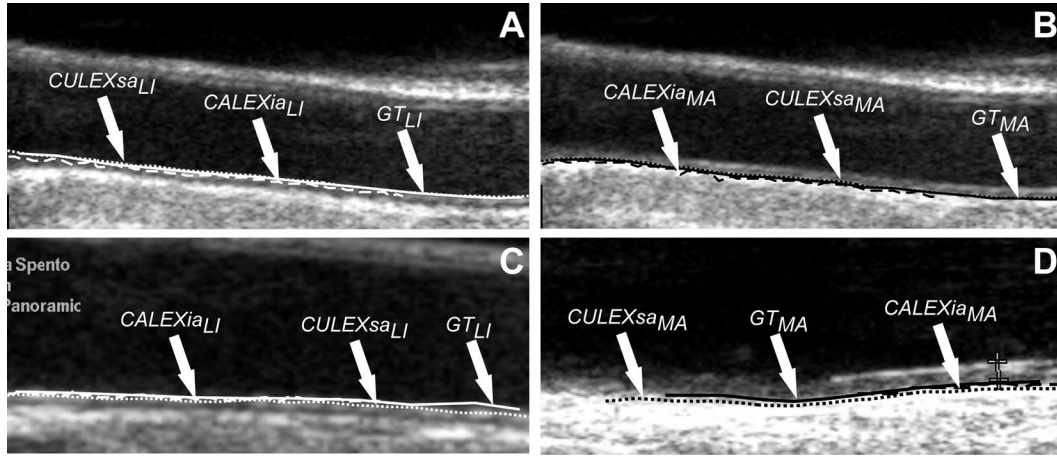
Fig. 8. Comparative samples of CALEXia (dashed lines) and CULEXsa (dotted lines) segmentation compared with GT (continuous lines). The top row contains images in which CULEXsa outperforms CALEXia; in the bottom row CALEXia outperforms CULEXsa. The left column [(A) and (C)] cmopares LI tracings (white lines); the right column [(B) and (D)] compares MA (black lines). (A) CULEXsa outperforms CALEXia in LI tracing. (B) CULEXsa outperforms CALEXia in MA tracing. (C) CALEXia outperforms CULEXsa in LI tracing. (D) CALEXia outperforms CULEXsa in MA tracing.

TABLE I. Mean Absolute Errors and Standard Deviations Calculated on the Image Database for the Two Segmentation Techniques.

Errors	Units	CALEXia	CULEXsa
Lumen-Intima (LI)	pixel	1.46 ± 1.51	0.55 ± 0.51
	mm	0.091 ± 0.093	0.035 ± 0.032
Media-Adventitia (MA)	pixel	0.40 ± 0.87	0.59 ± 0.46
	mm	0.025 ± 0.055	0.037 ± 0.029
Intima-Media Thickness (IMT)	pixel	0.87 ± 0.56	0.12 ± 0.14
	mm	0.054 ± 0.035	0.01 ± 0.01

The number of images used is 182. The first two rows report the mean absolute error for the LI interface; the next two rows report the mean absolute error for the MA interface. The last two rows report the IMT calculation errors. The axial resolution is 0.0625 mm/pixel.

for CULEXsa. Table I summarizes the mean absolute segmentation errors for the LI and MA interfaces expressed in pixels and millimeters for CALEXia and CULEXsa.

On the lumen-intima (LI) interface, the segmentation error of CALEXia $\left(\varepsilon^i_{\mathrm{CALEXia}_{\mathrm{LI}}}\right)$ is greater than that of CULEXsa $\left(\varepsilon^i_{\mathrm{CALEXia}_{\mathrm{LI}}}\right)$ (paired Student's t-test, $P < 0.05$). The segmentation of the LI interface is the most critical to CALEXia. This is due to the fact that the fuzzy K-means classifier, which we use to mark the transitions between lumen and intima [Fig. 4(d)], underestimates the LI position. The CALEXia average error on the LI interface is the only case in which we experienced segmentation errors greater than 1 pixel. The histogram is shown in Fig. 6(a) clearly demonstrates that the errors on the LI interface are between 1 and 2 pixels in about 70% of the 9100 points. To test possible improvement on the LI interface tracing, we experimented with different classifiers. In some cases, a better estimation of the LI position caused a detriment in the estimation of the MA position. This paper reports the optimal performance achieved. Some efficient classifiers require the selection of a threshold or critical value, but because complete automation a fundamental requirement of CALEXia, we preferred to rely on the automation ensured by K-means.

We found that in about 7% of the columns of the ROI, the K-means classifier could not cluster the signal envelope in three contiguous classes. Because the average ROI extension is about 300 columns, we had to discard on average 20 columns per ROI. In the worst case, 15% of the columns were discarded (corresponding to about 45 columns). Even considering column downsampling, we discarded less than 5 columns from a total number of 30 in the worst case. Therefore, the low number of K-means failures did not influence the accuracy of the system. Presently, we are working on trying to improve this part of the algorithm by adding intelligent and adaptive procedures to the clustering of each signal envelope.

For the media-adventitia (MA) interface, CALEXia showed an average error (0.40 ± 0.87 pixels) lower than CULEXsa (0.59 ± 0.46 pixels). Fig. 7 shows the superior performance of CALEXia on the MA interface.

Fig. 8 shows samples of CALEXia and CULEXsa tracings: the top row [Fig. 8(a) and 8(b)] shows samples in which CULEXsa outperforms CALEXia; the bottom row [Fig. 8(c) and 8(d)] shows samples in which CALEXia outperforms CULEXsa. The left column [Fig. 8(a) and 8(c)] shows the LI segmentation; whereas the right column [Fig. 8(b) and 8(d)] shows the MA. In Fig. 8(a),
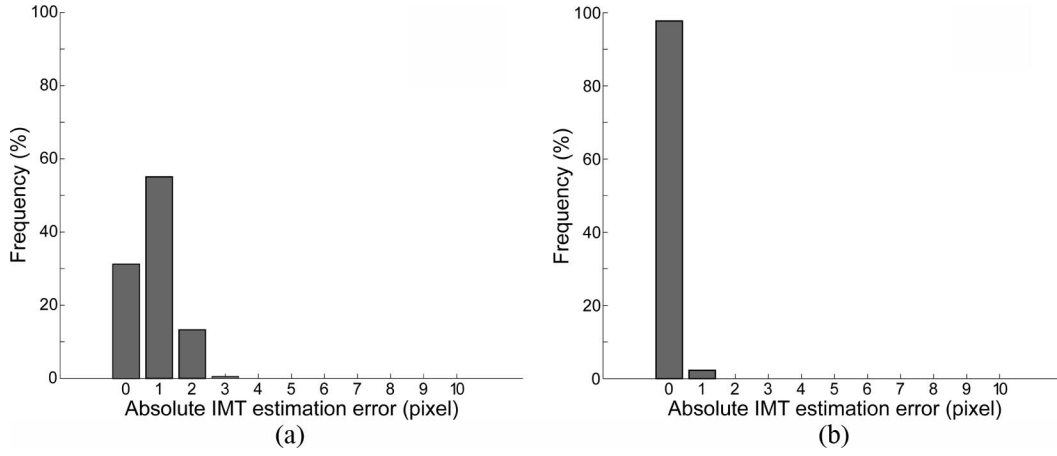
Fig. 9. Absolute IMT error distributions for CALEXia and CULEXsa. The 9100 error values (50 points × 182 images) are grouped in classes of 1 pixel each. The horizontal axis reports the absolute error in pixels. The vertical axis reports the relative frequency (i.e., the number of points falling in each class expressed as a percentage of the total number of error values). (a) Distribution of the $\varepsilon^i_{\text{CALEXia}_{\text{IMT}}}$. (b) Distribution of the $\varepsilon^i_{\text{CULEXsa}_{\text{IMT}}}$.

the LI profile traced by CULEXsa (white dotted line, CULEXsa$_{\text{LI}}$) is very close to ground truth (white continuous line, GT$_{\text{LI}}$), whereas the CALEXia tracing (white dashed line, CALEXia$_{\text{LI}}$) is clearly placed below GT$_{\text{LI}}$. In Fig. 8(b), CALEXia underestimates the MA boundary and its tracing (black dashed line, CALEXia$_{\text{MA}}$) is placed below the ground truth (black continuous line, GT$_{\text{MA}}$), whereas CULEXsa (black dotted line, CULEXsa$_{\text{MA}}$) traces a MA contour almost overlapped to GT_{MA}. In Fig. 8(c) CULEXsa$_{\text{LI}}$ is placed below GT_{LI} whereas CALEXia$_{\text{LI}}$ is overlapped to ground truth; in Fig. 8(d) because of the high echogenicity of the adventitia layer, CULEXsa$_{\text{MA}}$ is underestimated and CALEXia$_{\text{MA}}$ is better traced.

B. Percent Statistic Test

Considering $n = 3$ and $n = 182$; we obtained $P = 0.5$ and $\theta = 0.073$. Therefore, considering $\alpha = 0.05$, the percent statistic test is passed when $Z_0 > 0.427$. CALEXia showed a Z_0 score equal to 0.425 for the LI interface and of 0.578 for the MA interface. CULEXsa showed Z_0 scores of 0.499 for the LI and 0.564 for the MA.

CALEXia did not pass the percent statistic test when tracing the LI profile. As we will discuss in the following, this is due to the algorithm's underestimation of the LI interface. All of the remaining Z values were higher than the critical value. In all of these cases we can conclude that, from a statistical point of view, our techniques behave like a human operator in segmenting the carotid wall. More specifically, this test revealed that the distance of the computer-generated tracings from the average of the human operators is not statistically higher than the inter-observer variability, i.e., the variability of independent expert operators segmenting the image database.

C. IMT Measurement Error

For each image, we calculated the error in the IMT measurement according to (4). Again, we first computed

the common support between the GT, CALEXia, and CULEXsa tracings, and then we calculated the IMT error in 50 equally spaced points per image. We computed 9100 values of $\varepsilon^i_{\text{CALEXia}_{\text{IMT}}}$ and $\varepsilon^i_{\text{CALEXia}_{\text{IMT}}}$. Fig. 9 reports the histograms of the distribution of $\varepsilon^i_{\text{CALEXia}_{\text{IMT}}}$ and $\varepsilon^i_{\text{CALEXia}_{\text{IMT}}}$. The mean error for CALEXia is 0.87 ± 0.56 pixels, whereas that of CULEXsa is 0.12 ± 0.14 pixels. The average errors are, for both the techniques, less than 1 pixel. The IMT error values are reported in the third row of Table I.

CULEXsa offers better performances than CALEXia, showing a lower mean IMT error (paired Student's t-test, $P < 0.05$). The reason for this result is the imperfect segmentation of the LI interface traced by CALEXia. It can be noted, in fact, that the shape of the histogram in Fig. 9(a) is similar to that of Fig. 6(a). The segmentation error on the LI profile is reflected in the IMT estimation and makes the mean IMT error slightly lower than 1 pixel.

IV. Discussion

In this study, we characterized the performances of a new and completely automated technique for the segmentation of the CCA wall in longitudinal ultrasound images (CALEXia). This novel technique is based on an integrated approach consisting of feature extraction (required for seed points detection), line fitting (required to validate and connect line segments among them), and classification (used to select the correct line segments, as shown in Fig. 3). CALEXia showed robustness and effectiveness in automatically recognizing the CCA in the ultrasound image [12]. The principal aim of this paper is to show the extension of CALEXia that enables the carotid distal wall segmentation and computation of IMT measurement.

Among all the available techniques to perform automated IMT measurement, we chose to benchmark against a previous methodology we developed (CULEXsa). We

made this choice for two reasons. The first is that neither technique requires any user interaction to perform the image segmentation. After the images are acquired in DICOM format, both techniques yield LI, MA. and IMTs without the need of human intervention.

The second reason that we benchmarked against CULEXsa is that both the techniques were developed for working independently on data sets that were healthy carotids or on carotids with increased IMT value. In fact, we already demonstrated that our techniques could effectively process unhealthy diseased vessels [11], [12], [14], [19].

Another similarity between CALEXia and CULEXsa is that performance does not depend on the scanner settings. In clinical practice, the sonographer adjusts the system gains according to the specific patient. Different gains result in different contrast and brightness of the images. Being based only on relative thresholds, the performance of our techniques does not depend on the scanner type or settings. We already demonstrated that CULEXsa's performance does not depend on the ultrasound scanner used to acquire the images [14]. The CALEXia algorithm is based on an initial seed points detection and line segments tracing steps that require training [12]. To test the influence of the training set used on the system performance, we split the 200-image data set into 13 subsets of 15 randomly selected images each. Each subset (or trial run) was used to train CALEXia, thus resulting in 13 differently trained CALEXia systems. We computed the performance of each trial run and compared them. We showed that no trial run produced performance statistically different from the others. The overall system error, measured according to (4), ranged from 0.81 pixels to 0.93 pixels. Therefore, CALEXia also showed a good robustness to the training set used. Because the database used in this study consisted of images acquired from consecutive patients, with scanner settings that were different from subject to subject, we can conclude that our techniques' performance is independent of the system gains and scanner type.

In terms of LI and MA segmentation errors, the comparison of our results with previously published techniques is not straightforward. To our knowledge, the most performing techniques for IMT estimation did not characterize the segmentation performances of the single layers. Cheng *et al.*, who proposed a snake-based technique for the IMT measurement [7], characterized the segmentation performances of their technique on the LI and MA interfaces by comparing to human tracings on only 6 images. However, they only characterized in terms of root mean squared error (RMSE). Working with a spatial resolution equal to 0.096 mm, the RMSE measured by Cheng *et al.* was equal to 0.651 pixel (62.5 µm) for the LI interface and 0.402 pixel (38.6 µm) for the MA interface. We calculated the RMSE for CALEXia and found 1.31 pixels (81.9 µm) on the LI and 0.32 pixel (20.1 µm) on the MA interface. Thus, our technique showed lower RMSE values than Cheng *et al.*'s method when segmenting the MA

TABLE II. Intima-Media Thickness (IMT) Mean Values Calculated by the CALEXia and CULEXsa Techniques Compared With Ground Truth (GT).

$CALEXia_{IMT}$	$CULEXsa_{IMT}$	GT_{IMT}	Units
12.04 ± 6.17	14.09 ± 4.67	14.68 ± 4.71	pixel
0.75 ± 0.39	0.88 ± 0.29	0.92 ± 0.30	mm

The axial resolution is 0.0625 mm/pixel.

interface, but a higher RMSE error when segmenting the LI interface.

Fig. 9 reports the distribution of the IMT measurement errors. Again, CULEXsa offers better performances than CALEXia, showing a mean IMT error equal to 0.12 $\pm$ 0.14 pixel compared with 0.87 $\pm$ 0.56 for CALEXia (paired Student's t-test, $P < 0.05$). In IMT measurement, CALEXia is limited by its performance on LI segmentation, as previously mentioned.

However, the percent statistic test gave encouraging results. Particularly, CULEXsa passed the test for both the LI and MA interfaces, whereas CALEXia passed it when segmenting the MA, but not when segmenting the LI boundary. In this latter case, however, that the Z_0 score was equal to 0.425, against a critical value of 0.427. Therefore, we think that, despite the segmentation errors and the bias in the IMT measurement, the techniques are promising.

To further investigate the biases in the IMT estimation of the two methodologies, we reported the Bland-Altman plots. Preliminarily, we derived a single value of IMT for each image. This value was the average value of the 50 IMT estimates made on the image. We did the same also for manual tracings. Thus we obtained 182 IMT values for GT, CALEXia, and CULEXsa. Table II reports the average values of IMT measured on the sample database. It can be observed that both the techniques under-estimate the IMT value. Fig. 10 reports the Bland-Altman plots for CALEXia vs. GT [Fig. 10(a)] and CULEXsa vs. GT [Fig. 10(b)]. It is possible to observe the negative bias of the CALEXia estimates with respect to GT: Fig. 10(a) shows a mean value on the vertical axis equal to −2.35 pixel (about −147 µm). The bias of CULEXsa is greatly reduced and equal to −0.48 pixel (−30 µm). The best-performing algorithm that we found in literature for IMT estimation showed a bias equal to −1 µm [20], even though most of the techniques showed bias of about −10 µm [8]. Therefore, our methodologies provided IMT estimates with a higher bias. However, the cited algorithms required human interaction to select the portion of the image from where to start segmenting and measuring IMT.

The selection of the image portion in which IMT estimation is to be performed is crucial. In 2009, Loizou *et al.* [16] demonstrated that a snake-based segmentation procedure could be very effective in aiding the human operator in measuring the intima and media thicknesses. Their methodology was intended as a computer aid to atherosclerosis assessment. The operator could select the por-
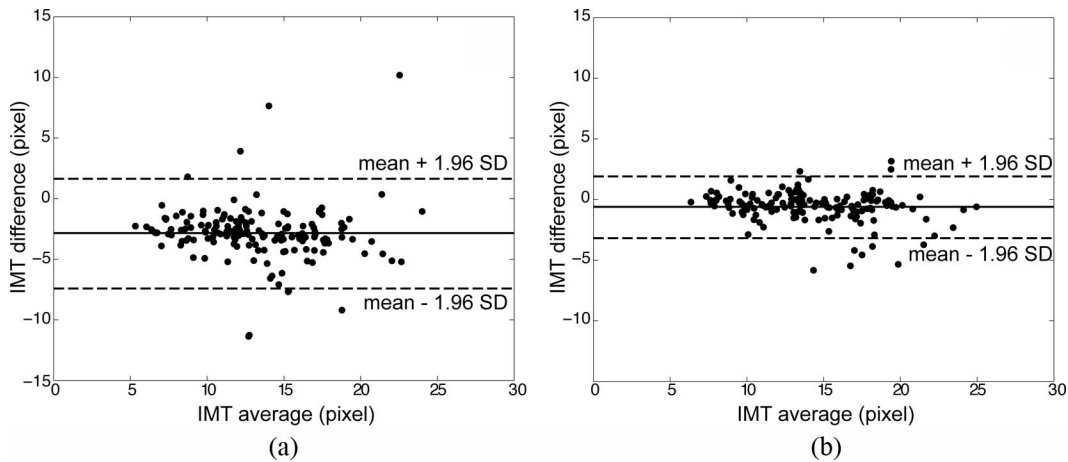
Fig. 10. Bland-Altman plots of the IMT measurement performed by CALEXia and CULEXsa compared with GT. Each circle represents an image from the database. The dotted line represents the average value of the estimate differences (i.e., of the quantity on the vertical axis); the dashed lines represent the mean value ± one standard deviation. The horizontal axis reports the average between the method's estimates and GT; the vertical axis the difference. It is possible to observe a negative mean value, which indicates an underestimation of IMT by the method. (a) CALEXia, (b) CULEXsa.

tion of the CCA distal wall and the algorithm then performed the measurement. This algorithm can therefore be thought as semi-automatic. We tested whether the region selection could impact the IMT measurement of CALEXia and CULEXsa. According to [16], a trained sonographist manually selected a rectangular region of interest placed on the distal wall, in a region of the image free from backscattering, excessive noise, and artifacts. The length of the ROI was fixed to 9 mm (i.e., 144 pixels) for all the images. Then we ran our IMT measurement procedure in that region only. The CALEXia mean IMT error was reduced to 0.33 ± 0.23 pixel (originally it was 0.87 ± 0.56), whereas CULEXsa did not show significant performance variations. In this condition, CALEXia showed performances comparable to other user-driven techniques [5], [7], [16], [21].

Like all the other proposed methodologies, our techniques also underestimate IMT.

There are two factors limiting the CALEXia performance: 1) the underestimation of the LI interface (as discussed previously), and 2) the segmentation of image regions characterized by a very low SNR. The solution of the two problems is not straightforward. Our aim is to improve the segmentation performances without losing the versatility of the algorithm. In fact, this is a generalized technique that, making use of a superior integrated architecture, is effective in processing almost any kind of image. The robustness to noise is good, because only 5% of the randomly selected images were incorrectly processed. Our methodology is effective in coping with different anatomies, because it can also process carotids that are not horizontal in the image, as well as curved arteries.

Finally, the major advantage of CALEXia with respect to CULEXsa is the computational cost. Both the algorithms were implemented in MATLAB environment (TheMathworks, Natick, MA) on a dual 2.5-GHz G5 PowerPC equipped with 4 GB of RAM. The average processing time for CALEXia was 3 s; that of CULEXsa was 32 s.

CALEXia, therefore, can be a suitable algorithm for quasi real-time processing.

V. Conclusions

We developed a completely user-independent algorithm for layers extraction of the carotid artery wall in ultrasound images. This novel technique (CALEXia), which represents a further step in carotid automated ultrasound image processing, was used to measure the IMT and was compared with a previously developed methodology. The data analysis of the segmentation and IMT measurement errors showed that the tracing of the LI boundary might have a scope of improvement. The underestimation of the IMT value depends on the quality of the LI tracing. Despite having a small challenge estimating LI, CALEXia out-performed CULEXsa in segmenting the MA interface. Also, we showed that by reducing the IMT measurement to a small portion of the image (as usually happens with user-driven techniques), performances become comparable to previously published non-automated methodologies.

CALEXia was developed taking into considerations all the variability sources, therefore it may represent a generalized and standard methodology toward completely automated and accurate IMT measurement. The authors are creating new databases from multiple institutions to validate their technologies. Also, they are working toward further improvement of the segmentation performances (by the fusion of CALEXia and CULEXsa using greedy techniques).

Giustetto (Visiting Scientist, Gradenigo Hospital, Torino, Italy) for her help in manual segmentation.

References

[1] M. W. Lorenz, H. S. Markus, M. L. Bots, M. Rosvall, and M. Sitzer, "Prediction of clinical cardiovascular events with carotid intima-media thickness: A systematic review and meta-analysis," *Circulation*, vol. 115, no. 4, pp. 459–467, Jan. 30, 2007.

[2] M. Rosvall, L. Janzon, G. Berglund, G. Engström, and B. Hedblad, "Incidence of stroke is related to carotid IMT even in the absence of plaque," *Atherosclerosis*, vol. 179, no. 2, pp. 325–331, Apr. 2005.

[3] E. de Groot, S. I. van Leuven, R. Duivenvoorden, M. C. Meuwese, F. Akdim, M. L. Bots, and J. J. Kastelein, "Measurement of carotid intima-media thickness to assess progression and regression of atherosclerosis," *Nat. Clin. Pract. Cardiovasc. Med.*, vol. 5, no. 5, pp. 280–288, May 2008.

[4] P. J. Touboul, P. Prati, P. Y. Scarabin, V. Adrai, E. Thibout, and P. Ducimetière, "Use of monitoring software to improve the measurement of carotid wall thickness by B-mode imaging," *J. Hypertens. Suppl.*, vol. 10, no. 5, pp. S37–S41, Jul. 1992.

[5] M. A. Gutierrez, P. E. Pilon, S. G. Lage, L. Kopel, R. T. Carvalho, and S. S. Furuie, "Automatic measurement of carotid diameter and wall thickness in ultrasound images," *Comput. Cardiol.*, vol. 29, pp. 359–362, 2002.

[6] Q. Liang, I. Wendelhag, J. Wikstrand, and T. Gustavsson, "A multiscale dynamic programming procedure for boundary detection in ultrasonic artery images," *IEEE Trans. Med. Imaging*, vol. 19, no. 2, pp. 127–142, Feb. 2000.

[7] D. C. Cheng, A. Schmidt-Trucksäss, K. S. Cheng, and H. Burkhardt, "Using snakes to detect the intimal and adventitial layers of the common carotid artery wall in sonographic images," *Comput. Methods Programs Biomed.*, vol. 67, no. 1, pp. 27–37, Jan. 2002.

[8] C. P. Loizou, C. S. Pattichis, M. Pantziaris, T. Tyllis, and A. Nicolaides, "Snakes based segmentation of the common carotid artery intima media," *Med. Biol. Eng. Comput.*, vol. 45, no. 1, pp. 35–49, Jan. 2007.

[9] S. Golemati, J. Stoitsis, E. G. Sifakis, T. Balkizas, and K. S. Nikita, "Using the Hough transform to segment ultrasound images of longitudinal and transverse sections of the carotid artery," *Ultrasound Med. Biol.*, vol. 33, no. 12, pp. 1918–1932, Dec. 2007.

[10] S. Delsanto, F. Molinari, P. Giustetto, W. Liboni, S. Badalamenti, and J. S. Suri, "Characterization of a completely user-independent algorithm for carotid artery segmentation in 2-D ultrasound images," *IEEE Trans. Instrum. Meas.*, vol. 56, no. 4, pp. 1265–1274, 2007.

[11] F. Molinari, S. Delsanto, P. Giustetto, W. Liboni, S. Badalamenti, and J. S. Suri, "User-independent plaque segmentation and accurate intima-media thickness measurement of carotid artery wall using ultrasound," in *Advances in Diagnostic and Therapeutic Ultrasound Imaging*, J. S. Suri, R. F. Chang, C. Kathuria, F. Molinari, and A. Fenster, eds., Norwood, MA: Artech House, 2008, pp. 111–140.

[12] F. Molinari, G. Zeng, and J. S. Suri, "An integrated approach to computer- based automated tracing and its validation for 200 common carotid arterial wall ultrasound images: A new technique," *J. Ultrasound Med.*, vol. 29, no. 3, pp. 399–419, 2010.

[13] E. Kyriacou, M. S. Pattichis, C. I. Christodoulou, C. S. Pattichis, S. Kakkos, M. Griffin, and A. Nicolaides, "Ultrasound imaging in the analysis of carotid plaque morphology for the assessment of stroke," *Plaque Imaging: Pixel to Molecular Level*, J. S. Suri, C. Yuan, D. L. Wilson, and S. Laxminarayan, eds., Amsterdam: IOS Press, 2005, pp. 241–275.

[14] F. Molinari, W. Liboni, P. Giustetto, S. Badalamenti, and J. S. Suri, "Automatic computer-based tracings (ACT) in longitudinal 2-D ultrasound images using different scanners," *J. Mech. Med. Biol.*, vol. 9, no. 4, pp. 481–505, 2009.

[15] D. J. Williams and M. Shah, "A fast algorithm for active contours and curvature estimation," *CVGIP: Image Underst.*, vol. 55, no. 1, pp. 14–26, Jan. 1992.

[16] C. P. Loizou, C. S. Pattichis, A. N. Nicolaides, and M. Pantziaris, "Manual and automated media and intima thickness measurements of the common carotid artery," *IEEE Trans. Ultrason. Ferroelectr. Freq. Control*, vol. 56, no. 5, pp. 983–994, May 2009.

[17] V. Chalana and Y. Kim, "A methodology for evaluation of boundary detection algorithms on medical images," *IEEE Trans. Med. Imaging*, vol. 16, no. 5, pp. 642–652, Oct. 1997.

[18] C. Alberola-López, M. Martin-Fernandez, and J. Ruiz-Alzola, "Comments on: A methodology for evaluation of boundary detection algorithms on medical images," *IEEE Trans. Med. Imaging*, vol. 23, no. 5, pp. 658–660, May 2004.

[19] F. Molinari, W. Liboni, E. Pavanelli, P. Giustetto, S. Badalamenti, and J. S. Suri, "Accurate and automatic carotid plaque characterization in contrast enhanced 2-D ultrasound images," *Conf. Proc. IEEE Eng. Med. Biol. Soc.*, vol. 2007, pp. 335–338, 2007.

[20] F. Faita, V. Gemignani, E. Bianchini, C. Giannarelli, L. Ghiadoni, and M. Demi, "Real-time measurement system for evaluation of the carotid intima-media thickness with a robust edge operator," *J. Ultrasound Med.*, vol. 27, no. 9, pp. 1353–1361, Sep. 2008.

[21] P. Pignoli and T. Longo, "Evaluation of atherosclerosis with B-mode ultrasound imaging," *J. Nucl. Med. Allied Sci.*, vol. 32, no. 3, pp. 166–173, Jul.-Sep. 1988.

Filippo Molinari was born in Piacenza, Italy. He received the Italian Laurea degree and the Ph.D. in electronics from the Politecnico di Torino, Torino, Italy, in 1997 and 2000, respectively. Since 2002, he has been Assistant Professor on faculty of the Department of Electronics of the Politecnico di Torino. Since 2001, he has taught courses on biomedical signal processing, biomedical image processing, and instrumentation for medical imaging. His research topics include the analysis of biosignals and the biomedical image processing applied to the computer-aided diagnosis and therapy. In the field of ultrasound imaging, Dr. Molinari developed diagnosis procedures for vascular applications and thyroid assessment. Dr. Molinari is a member of the IEEE Engineering in Medicine and Biology Society (EMBS), of the Italian Group of Bioengineering (GNB), and of the American Institue for Ultrasound in Medicine (AIUM).
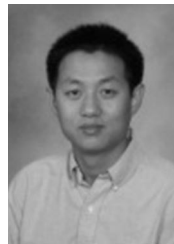
Guang Zeng received the B.S. degree from Xiangtan University, China in 1998. He received the M.S. degree in 2005 and the Ph.D. degree in 2008 from Clemson University, SC, both in Electrical Engineering. He is currently working in the Aging and Dementia Imaging Research Laboratory, Mayo Clinic, Rochester, MN. His research interests include biomedical image processing, pattern recognition, and computer vision.

Jasjit S. Suri received his Master's degree from the University of Illinois, Chicago, his doctorate from the University of Washington, Seattle, and his executive management degree from Weatherhead School of Management, Case Western Reserve University, Cleveland. He is an innovator, visionary, scientist, and an internationally known world leader, has spent over 25 years in the fields of biomedical engineering and sciences and their management. During his career in biomedical industry and imaging, he has had increasing growth and responsibilities from scientific Engineer, Scientist, Manager, Director R&D, Senior Director, and Vice President, to Chief Technology Officer-level positions in companies like Siemens Medical Systems, Philips Medical Systems, Fisher Imaging Corporation, Eigen Inc., and Biomedical Technologies, and he managed up to 100 people. Dr. Suri has written more than 300 publications including US and European patents, papers in peer-reviewed journals and conference proceedings, and book chapters. His major contributions are in the areas of diagno-

sis and therapeutic devices covering the heart, brain, spine, thyroid, eye, vasculature, breast, and prostate. He has championed the field of image segmentation and registration for image-guided surgical applications. During his leadership, he has released over six different products along with the FDA approvals for products such as Voyager, SenoScan, and Artermis.

Dr. Suri has been board member of several international journals and conference committees. Dr. Suri was awarded the President's Gold medal in 1980 and the Fellow of the American Institute of Medical and Biological Engineering (AIMBE), awarded by the National Academy of Sciences, Washington, DC in 2004. Dr. Suri has been the chairman of the IEEE Denver section and has won more than 50 awards during his career.